Theoretical modeling of vertical-cavity surface-emitting lasers with polarized optical feedback

P. Besnard, F. Robert, M. L. Charès, and G. M. Stéphan*
ENSSAT, Laboratoire d'Optronique associé au CNRS (UPRESA6082), GISO2, 6 rue de Kérampont, 22305 Lannion, France
(Received 21 March 1997)

Vertical-cavity surface-emitting lasers have two preferential polarization states related to the crystal axes of the quantum wells. In this work, we consider such a laser extended by means of a polarizer inserted in an external cavity. When the phase of the external-cavity field is modulated, the laser switches from one polarization state to the other. Experimental and theoretical results in which spin interactions are inserted are presented and discussed. A linear stability analysis is applied to the two linearly polarized stationary states in the case of structures with small amplitude anisotropies. It shows how the phase of the reinjected field affects the stability of the mode. Coefficients for gain compression and spontaneous noise are mandatory to obtain polarization flips in the simulations. [S1050-2947(97)02810-2]

PACS number(s): 42.60.Mi, 42.65.−k, 42.55.Px, 42.55.Sa

I. INTRODUCTION

Polarization properties of laser light have been a topic of research since the discovery of the laser [1]. Until now it has not been used in coherent communication systems because the polarization state is lost during the propagation along the fiber. Nevertheless, a polarization-bistable laser diode could have some advantages over direct bias modulation such as less power dissipation, a high contrast ratio, or less frequency chirp. Chen and Liu [2] have already proposed such a scheme for optical logical gates [3] which could present better suitability for cascading [4] (see Fig. 1). Unfortunately, components used in this study were not reproducible. Seemingly, identical structures do not always exhibit bistability. Later, reliable bistable devices have been produced. (1) Klehr *et al.* [5] obtained TE-TM modulation up to 8 GHz with a strained ridge waveguide in InGaAsP InP lasers. (2) Ouchi *et al.* [6] fabricated bielectrode $Al_xGa_{1-x}As$ GaAs distributed feedback lasers with TE-TM polarization switching between two longitudinal modes. Control of the bias current in each electrode enables the polarization state to switch and moreover to tune the lasing wavelength.

In these studies, the polarization state was switched by changing the bias current. Some researchers proposed other ways to control the TE-TM switching: (1) use of an external electric field [7] in a tensile-strained quantum-well laser, (2) use of a saturable absorbing layer [8], (3) use of injection from an external radiation [9,10], and (4) use of an extended cavity [11–13]. In this last case, the modulation was brought by an electro-optic modulator. Toda, Ogasaware, and Ito [14] explained this setup by analyzing the net gain of the two orthogonal modes. Choquette *et al.* [15] and Pan, Jiang, and Dagenais [16] proposed to use cruciform vertical-cavity laser diodes. One difference between vertical-cavity surface-emitting laser (VCSEL) and conventional laser structures rests on their respective anisotropies. The latter generally have a large anisotropy between the TE and TM modes because of the asymmetry of the active zone. They always work on the same polarization and this is why one can characterize them by the expression ''scalar laser.'' This anisotropy could be compensated using an antireflection coated laser submitted to optical polarized feedback [14]. In fact, there are different origins to anisotropies: (1) the host medium (due to macroscopic stress, temperature effects, or gain profiles, etc.), (2) the geometry of the optical waveguide, (3) the linear microscopic properties of the physical system interacting with light (optical dipoles), (4) the saturation effect, and (5) the feedback light or external constraint. In a VCSEL, the light is emitted along a direction perpendicular to the junction or to the quantum wells of the gain region. The anisotropy is very weak and the polarization is along the preferential axes [110] or [1$\bar{1}$0] for components grown on (001) substrates. These nearly degenerate orthogonal linearly polarized eigenstates lead to a certain randomness in the direction of polarization which is not well defined (along [110] or [1$\bar{1}$0]) from one component to another. It could be a main drawback as the control of the polarization properties is important for polarization-sensitive applications. It can also be turned into an advantage if we know how to control it. To sum up, VCSELs are lasers with weak anisotropies and able to work on several polarization states. One could thus speak of *vectorial lasers*. This vectorial nature is the cause of an intensity noise increase [17,18] or polarization instabilities [19]. Several techniques have been proposed to control the

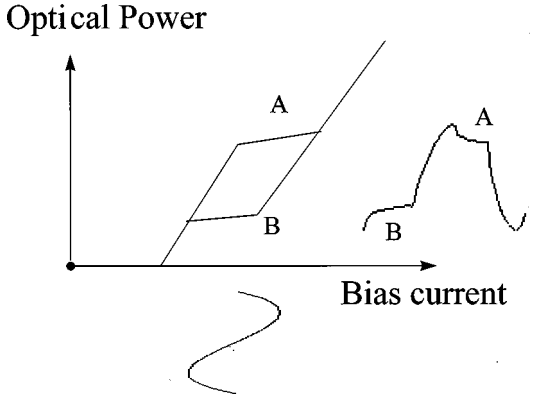

FIG. 1. Simple image showing how to modulate a signal using bistability.

*Electronic address: besnard@enssat.fr

VCSEL polarization state. Most of the schemes rely on breaking the symmetry in the plane of the quantum wells during the process of fabricating the lasers: (1) use of polarization properties of VCSELs which depends upon the gain [20], (2) use of an anisotropic laser mirror [21,22], (3) use of a misoriented substrate [23], (4) use of an anisotropic gain distribution in [110]-oriented strained quantum-well structures [24], and (5) use of asymmetric structures [25,26].

The other way to control the polarization of the laser light is the polarized optical feedback (POF) method. Here, one takes advantage of the weak anisotropy of the VCSELs by breaking the symmetry from the outside. Previous works have shown [27–30] that in the case of a single-frequency laser with weak anisotropies, it is possible to control the polarization state by changing the phase difference between the laser field and the external field. In the case of VCSELs this phase can be scanned by changing the external-cavity length or the laser frequency. This last parameter can be modulated through the bias current (chirp effects).

In Sec. II we describe our experimental results using a VCSEL submitted to polarized optical feedback. In Sec. III the model introduced in [31] is used to understand the effect of an extended cavity. In order to describe theoretically these experiments, the vectorial nature of the laser should be taken into account. Both orthogonal modes with a detailed description of the associated quantum transitions [27,31] are included. In this model, the laser works at line center and anisotropies originating from the gain profile are not taken into account. With these assumptions, in most cases, there are two stationary states which are linearly polarized. We develop a linear stability analysis of these states in order to study the effect of a weak feedback in the case of VCSELs. The optical feedback can make the laser bistable with the optical phase of the external field as the control parameter. In Sec. IV numerical investigations indicate that only one linearly polarized mode will survive in the bistable regime. These results show that the control of polarization state of the laser can be well simulated.

II. EXPERIMENT

A. Experimental arrangement

We use commercially available components emitting at 850 nm. The devices have one wavelength cavity with four GaAs quantum wells. Their threshold currents are 2.3–2.5 mA and operate at a single frequency for normalized bias currents between 1.0 and $\cong 1.8$. Commercial drivers are used for the temperature stabilization and the injection current. Modulation of the current was performed by an uhf generator when needed. Two Fabry-Pérot interferometers [one with 10-GHz free spectral range (FSR) and a finesse of 150 and another with variable FSR and a finesse greater than 50], a fast oscilloscope, an optical spectrum analyzer, and a rf spectrum analyzer allow for signal analysis.

Figure 2 shows the experimental arrangement. A polarizer P_f is inserted in the extended cavity. The feedback light is polarized along the direction (Y) perpendicular to the polarization of the free-running laser (mode X). P_a controls its amplitude. A piezoelectric ceramic (PZ) can change the length L of the external cavity. A polarizing cube beam splitter P_d and a half-wave plate allow for the detection of the signal along the two eigenaxes of the bare laser.

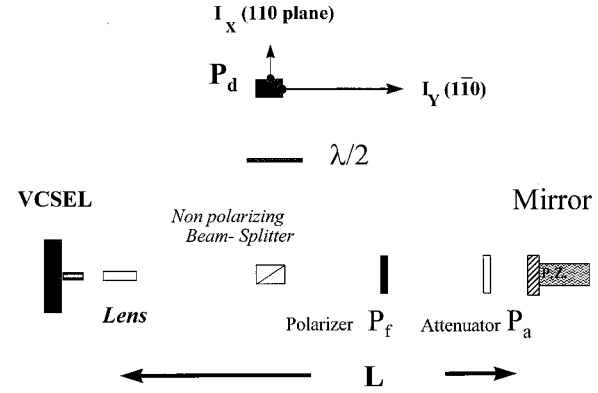

FIG. 2. Schematic representation of the experimental setup. The mirror is mounted on a piezoelectric ceramic. The polarizer P_f is oriented along the direction Y, perpendicular to the polarization of the laser without feedback (X).

B. Numerical values

We have summed up the parameter values of the VCSELs in Table I. If the surface S of the four quantum wells is equal to 78.5×10^{-12} m^2 and the thickness of a quantum well L_{QW} is equal to 10 nm, then the theoretical currents at transparency J_0 and at threshold J_{th} are given by

$$J_0=\frac{e4L_{\mathrm{QW}}S}{\rho_i\tau_e}N_0=1.26\ \mathrm{mA},\quad J_{\mathrm{th}}=\frac{e4L_{\mathrm{QW}}S}{\rho_i\tau_e}N_{\mathrm{th}}=2.75\ \mathrm{mA},$$

where e is the electron charge and ρ_i the internal quantum efficiency. τ_e is relaxation time of the total carrier number. The carrier density at threshold is then given by $N_{\mathrm{th}}=N_0+1/\Gamma G_N\tau_p$ where τ_p is the photon lifetime and N_0 the carrier density at transparency. Γ is the confinement factor ($=0.05$) including the weak thickness of the quantum wells. G_N is the differential gain (m^3 s^{-1}). Some parameters, such as Henry's factor α, were deduced by different measurements (linewidth versus bias current, oscillation frequency versus bias current using modulation techniques, frequency shift versus feedback strength). Other parameters were reported from the literature [32]. As the polarization state can be controlled, the frequency splitting between orthogonal modes is easily measured [30]: it is in the range 10–20 GHz for our lasers. No switching between the two polarization states, as described in [33] and in [34], is observed in the light-intensity curves. This is in agreement with theoretical results given in [34].

C. Control of the polarization state

The description of our results has already been given in [35]. Feedback phenomena could give rise to numerous effects in conventional lasers [36] and this optical perturbation is known to affect the laser properties [37,38]. Several studies have been made to understand the dynamics of such

TABLE I. Parameter values used in the theoretical analysis.

Meaning	Parameter	Numerical value
Laser cavity length	L_d	1 μm
Diameter		10 μm
Output coupling laser mirror	$r_2(r_1=99.95\%)$	99.75%
Internal quantum efficiency	ρ_i	0.7
Cavity lifetime	τ_c	26.6 fs
Phase index	n_ϕ	3.6
Group index	n_g	4
Absorption losses	α_a	10 cm^{-1}
Mirror losses	$\alpha_M=(L_d)^{-1}\ln[(r_1r_2)^{-1}]$	30 cm^{-1}
Photon lifetime	$\tau_p=(V_g\alpha_t)^{-1}$	3.3 ps
Differential gain	G_N	2.9×10^{-12} m^3 s^{-1}
Confinement factor	Γ	0.05
Carrier density at transparency	N_0	1.75×10^{24} m^{-3}
Carrier density at threshold	$N_{\rm th}=N_0+(\Gamma G_N\tau_p)^{-1}$	3.8×10^{24} m^{-3}
Carrier lifetime	τ_e	1 ns
Spin relaxation lifetime	τ_s	10 ps
Linewidth enhancement factor	α	3.8
Spontaneous emission factor	β	2×10^{-3}

coupled cavities [39,40]. Different regimes are defined according to the power of the reinjected light. Therefore one would usually try to design feedback-insensitive lasers [41].

In our case, one has to consider the vectorial nature of VCSELs. The solitary laser oscillates on a single transverse-longitudinal mode (X) for any value of the injection current. The inherent anisotropy of the free-running laser is small. The laser submitted to the feedback field which is linearly polarized along Y oscillates along Y or X following the phase of this field.

The feedback strength does not need to be strong in order to compensate for the internal anisotropy. The effective reflectivity r_3 of the external cavity has been deduced from the measurements of the shift of the optical frequency. r_3 is between 10^{-3} and a few 10^{-2} in the experiment. It follows that the laser oscillates in the first or second region of the Tkach-Chraplyvy classification [42].

The effective losses of the perpendicular mode Y are dependent upon the phase ψ of the external field. ψ governs the interference between the internal laser field and the feedback field. When this interference is positive the laser tends to oscillate with the Y polarization. Two control parameters may be used to command $\psi=4\pi L/\lambda=\omega\tau$: the length L of the external cavity [29] or the frequency $\nu=\omega/2\pi$. Here we focus on the second method, which is based on the frequency chirp, linked to a variation of the injection current i_m. The laser frequency chirp produces a change in the phase of the feedback light ($\Delta\phi=4\pi(L/c)\Delta\nu$). Figure 3 shows the current of the VCSEL (upper trace i_m) and the output intensities I_X and I_Y as a function of time. The pump parameter i_m is modulated at 1 MHz. During a scan of the order of π, there is a polarization flip and I_Y is complementary to I_X. Switching between the X and Y modes has been obtained up to 30–50 MHz depending on the laser component. Above this value, the modulation depth has to be increased so much that the laser reaches values of the bias current where several transverse modes exist [35]. The polarization switches are then driven by partition noise and mode competition. This change of behavior can be explained by the transition from thermal effects towards carrier effects in the current-frequency transfer function [43]. In semiconductor lasers, a first plateau (thermal band) is in the range 1–100 MHz (Fig. 6 in Ref. [35]). The chirp for static measurements is higher in VCSELs (-320 GHz/mA) than in conventional lasers (-3 to -10 GHz/mA). It indicates the major importance of temperature effects in VCSEL (greater thermal resistance). Above the thermal band, the chirp is due to the electron-hole pairs (electronic band) so that in this region, the response is the same as the one encountered in conventional lasers. In the thermal band, this transfer function explains why a small voltage amplitude could control the polarization as a small value is sufficient to let the phase scan a complete cycle [0:2π]. At 1 MHz, this voltage amplitude is as small as -20.5 dBm. On the contrary, in the electronic band, the chirp is smaller and the modulation depth has to be increased

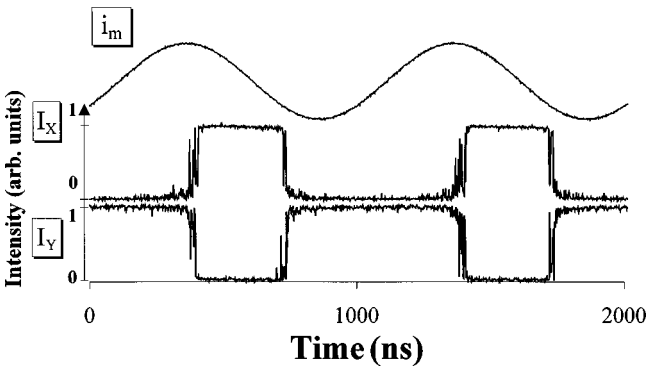

FIG. 3. Polarization switchings when bias current (upper trace) is modulated at 1 MHz with a modulation depth of -20.5 dBm. The optical power (lower trace) detected along x is off and on depending on the value of the phase. The complementary signal is obtained along y. The external cavity length is equal to 5 cm; $r_3=1\%$.

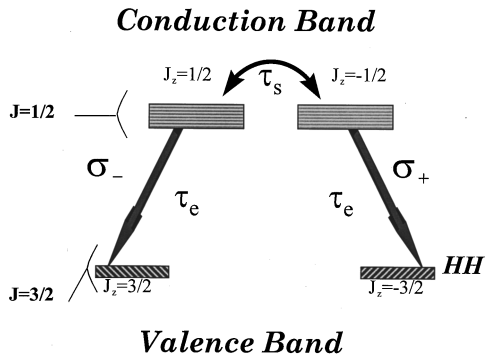

FIG. 4. Four-level model used in the theory.

with the consequences already mentioned.

The duration of the transition from one polarization state to another depends on f_m. Typical values are 10–30 ns for a modulation frequency of 1 Mhz. Note that with this method, the polarization state of the laser can be chosen for any bias current.

III. THEORY

In this paper we will focus the theoretical study on the influence of the external phase on the polarization stability of VCSELs. The other parameters will be considered as fixed.

A. Two-population model

A vectorial analysis of the field and the medium has been detailed in [34]. In this analysis, four levels have been taken into account as shown in Fig. 4. Transitions between the conduction band ($J_z=\pm\frac{1}{2}$) and the heavy-hole band ($J_z=\pm\frac{3}{2}$) are considered. In a first approximation, the light-hole band is considered out of resonance as the quantum-well structure lowers its energy. The dipole moment which links the sublevels $J_z=\frac{1}{2}$ to $\frac{3}{2}$ ($J_z=-\frac{1}{2}$ to $-\frac{3}{2}$) is coupled with the left (right) circularly polarized light. The two systems are coupled through spin relaxation. As the value of the associated time constant τ_s (10 ps) lies between the carrier relaxation time τ_s (1 ns) and the photon lifetime τ_p (3 ps), the equation for the population difference between the sublevels with opposite value of J_z cannot be adiabatically eliminated. The right and left circular fields are coupled to the medium through the total carrier density N and the difference S between the carrier densities with positive and negative values of J_z. *At line center*, these carrier density variables obey the following equations:

$$\frac{dN}{dt}=P-\frac{N}{\tau_e}-\Gamma G_N(1-\beta_- I_- -\theta_- I_+)(N-S-N_0)I_- -\Gamma G_N(1-\beta_+ I_+ -\theta_+ I_-)(N+S-N_0)I_+ , \quad (1)$$

$$\frac{dS}{dt}=-\frac{S}{\tau_s}+\Gamma G_N(1-\beta_- I_- -\theta_- I_+)(N-S-N_0)I_- -\Gamma G_N(1-\beta_+ I_+ -\theta_+ I_-)(N+S-N_0)I_+ . \quad (2)$$

P is the pump rate per unit volume ($P=\eta J/ed$ with J the bias-current density, d the thickness of the active zone, e the electron charge, η the quantum efficiency). $\tau_s(\gamma_s=1/\tau_s)$ is the relaxation time associated with spin relaxation. $I_{+(-)}$ is the photon density of the right (left) circular wave. Two slight modifications (see Appendixes A and B) have been brought to equations of Ref. [34]. The first one is the introduction of the carrier number at transparency N_0 as the notion of holes has been introduced. The second one is the insertion of self- and cross-gain-compression coefficients β_+, θ_+, β_-, θ_-. We have chosen to name them ''gain-compression'' factors instead of ''saturation'' factors to make a clear distinction with the saturation parameters usually defined in gas lasers and which are obtained by the adiabatic elimination of the population inversion variable. These compression terms are obtained in the scalar case by means of an exact elimination procedure for the polarization [44]. They may be derived from theoretical calculations [45]. In semiconductor lasers, the equation for the carriers (or the inversion) cannot be eliminated so that the saturation is contained in Eq. (1) without gain-compression terms. In this paper, the usual symbols for semiconductor lasers have been used.

Two equations will describe the evolution of the circular components $E_\pm$ of the field:

$$\dot{E}_\pm=-\frac{E_\pm}{2\tau_p}-i(\omega-\omega_t)E_\pm-(\gamma_a+i\gamma_b)E_\mp+\frac{1}{2}\Gamma G_N \times(1-\beta_\pm I_\pm-\theta_\pm I_\mp+i\alpha)(N\pm S-N_0)E_\pm , \quad (3)$$

with $|E_\pm|^2=I_\pm$, α is the linewidth enhancement factor. τ_p is the photon lifetime. It is related to the internal (α_a) and reflection losses (α_M): $1/\tau_p=v_g\alpha_t=(c/n_g)(\alpha_a+\alpha_M)$ where $\alpha_M=(1/L_d)\ln(1/r_1r_2)$. $r_1(=99.95\%)$, $r_2(=99.75\%)$ are the reflectivities of the laser mirrors. L_d is the effective laser-cavity length which is different from the geometrical length, as one should consider the penetration depth into the Bragg reflectors [46]. ω is the optical angular frequency resulting from the transition between the two bands, ω_t the angular frequency at transparency. γ_b is the birefringence and γ_a the anisotropic amplitude loss. $2(\gamma_b-\alpha\gamma_a)$ is the frequency splitting between the $\hat{x}$- ([110] or [110]) and $\hat{y}$-polarized solutions [34]. As has been shown in [34] for a free-running laser, many of the interesting phenomena of polarization switching can be explained as a consequence of birefringence and saturable dispersion. Conditions of bistability, monostability, and dynamical instabilities have been demonstrated [34] for the free-running laser. In our experiment, *the solitary laser is monostable* for one component, the polarization is locked onto a main axis by the anisotropy due to a residual stress. The saturable dispersion maintains emission onto one of the linear polarized states. The components have a small (often negligible) gain anisotropy together with the residual birefringence Δn which causes the two linear polarizations to have different frequencies. Typically, the splitting is 12 GHz (between 10 and 13 GHz), which gives $\Delta n=7\times10^{-5}$ or $\gamma_b=37.5$ GHz (between 31.4 and 41 GHz) if the amplitude anisotropy is taken equal to zero. However, the study will be devoted to the whole range of phase anisotropies. The different causes of the anisotropies are taken into account: the macroscopic host through its dichroism and birefringence (which will be represented, respectively, by γ_a

and γ_b), the microscopic medium through the spin interaction variable S, the compression of the gain (only in the numerical simulations) through $\beta_\pm$, $\theta_\pm$, and the feedback as developed in the next section.

B. Modeling the external cavity

The extended cavity is taken into account by replacing the scalar reflectivity r_2 of the output laser mirror by an equivalent reflectivity $\hat{r}_{\rm eff}$ [47]. Due to the vectorial nature of the problem, $\hat{r}_{\rm eff}$ is no longer a scalar symbol but becomes a vector:

$$\begin{pmatrix} r_{2\mathrm{eff}+}E_+ \\ r_{2\mathrm{eff}-}E_- \end{pmatrix} = r_2\begin{pmatrix} E_+ \\ E_- \end{pmatrix} + r_2 X \sum_{n=1}^{+\infty} (-r_2 r_3)^{n-1} \times \mathbf{M}_c^n e^{-in\omega\tau}\begin{pmatrix} E_+(t-n\tau) \\ E_-(t-n\tau) \end{pmatrix}, \tag{4}$$

where $\tau = 2L/c$ is the round-trip time, L is the external-cavity length, and $\mathbf{M}_c = \left(\begin{smallmatrix} m_+ & c_+ \\ c_- & m_- \end{smallmatrix}\right)$ is the Jones matrix [48] of the polarizer, expressed in the circular basis. $r_{2\mathrm{eff}\pm}$ represent the effective reflectivities of each polarized component of the field. We have assumed that the output mirror and the external mirror (reflectivity r_3) are isotropic and that $X = (r_3/r_2)(1-r_2^2) = 0.005 r_3$. For simplicity, diffraction losses are included in r_3. The second matrix term in Eq. (4) represents the total anisotropy induced by the external cavity. Its Hermitian part is associated with amplitude losses and its anti-Hermitian part with linear (birefringence) and circular phase anisotropies (circular dichroism).

After one round-trip, the matrix for an X polarizer is in the x,y basis: $\left(\begin{smallmatrix} 1 & 0 \\ 0 & 0 \end{smallmatrix}\right)$, whereas in the circular basis $\frac{1}{2}\left(\begin{smallmatrix} 1 & 1 \\ 1 & 1 \end{smallmatrix}\right)$. We will take in the following a Y polarizer and thus

$$\mathbf{M}_c = \frac{1}{2}\begin{pmatrix} 1 & -1 \\ -1 & 1 \end{pmatrix}.$$

The equivalent reflectivity will give rise to two complex photon lifetimes, one for each polarized mode:

$$\frac{1}{\tau_{p\pm}} = v_g\left[\alpha_a + \frac{1}{L_d}\ln\left(\frac{1}{r_1 r_{2\mathrm{eff}\pm}}\right)\right] = \frac{1}{\tau_p} - \frac{2}{\tau_c}\ln\left(\frac{r_{2\mathrm{eff}\pm}}{r_2}\right). \tag{5}$$

In Eq. (3), the following term becomes

$$\frac{E_\pm}{2\tau_{p\pm}} = \frac{E_\pm}{2\tau_p} - \frac{E_\pm}{\tau_c}\ln\left(\frac{r_{2\mathrm{eff}\pm}}{r_2}\right).$$

In this study $\|X\| < 10^{-5}$ and $\|r_2 r_3 \mathbf{M}_c e^{-i\omega\tau}\| < 5\times 10^{-2}$ so that *only one round-trip term will be considered*. $\ln(r_{2\mathrm{eff}\pm}/r_2)$ may be expanded into $r_{2\mathrm{eff}\pm}/r_2 - 1$ as long as $E_{+(-)}(t-\tau)$ are of the same order of magnitude as the delayed terms $E_+(t)$, $E_-(t)$:

$$\frac{1}{\tau_c}\begin{pmatrix} E_+\ln\left(\frac{r_{2\mathrm{eff}+}}{r_2}\right) \\ E_-\ln\left(\frac{r_{2\mathrm{eff}-}}{r_2}\right) \end{pmatrix} \approx \frac{1}{r_2\tau_c}\begin{pmatrix} r_{2\mathrm{eff}+}E_+ - r_2 E_+ \\ r_{2\mathrm{eff}-}E_- - r_2 E_- \end{pmatrix} = \frac{X}{\tau_c}\mathbf{M}_c e^{-i\omega\tau}\begin{pmatrix} E_+(t-\tau) \\ E_-(t-\tau) \end{pmatrix}.$$

Then Eq. (3) becomes

$$\begin{aligned} \dot{E}_\pm = {} & \frac{1}{2}\Gamma G_N(1+i\alpha)(N\pm S - N_{\rm th})E_\pm \\ & - \frac{1}{2}\Gamma G_N(\beta_\pm I_\pm + \theta_\pm I_\mp)(N\pm S - N_0)E_\pm \\ & - (\gamma_a + i\gamma_b)E_\mp + \frac{X}{\tau_c} m_\pm E_\pm(t-\tau)e^{-i\omega\tau} \\ & + \frac{X}{\tau_c} c_\pm E_\mp(t-\tau)e^{-i\omega\tau}, \end{aligned} \tag{6}$$

where, when the anisotropies are discarded, the carrier density and the angular frequency become at threshold

$$N = N_{\rm th} = N_0 + \frac{1}{\Gamma G_N \tau_p} \quad \text{and}$$

$$\omega = \omega_0 = \omega_t + \frac{\alpha}{2}\Gamma G_N(N_{\rm th} - N_0) = \omega_t + \frac{\alpha}{2\tau_p}.$$

The difference $\omega_0 - \omega_t = \alpha/2\tau_p$ is the frequency shift from transparency (the medium does not absorb at $N = N_0$) to threshold. This definition gives a reference frequency equal to zero at threshold, as we assume that above it, the carrier density and the laser frequency are clamped at $N = N_{\rm th}$ and at $\omega = \omega_0$.

C. Linear stability analysis

1. Solutions without feedback

We will look for stationary solutions for the field of the form $E_\pm = e_\pm e^{i(\Delta\omega_\pm t \pm \varphi)}$ with $\Delta\omega_\pm = \omega_\pm - \omega_0$. Stationary values for Eqs. (1), (2), and (6) are denoted N_s, S_s, ω_s, and $e_\pm$. A stationary solution will imply $\omega_+ = \omega_- = \omega_s$ with $\Delta\omega_\pm = \Delta\omega_s$ the deviation from the optical angular frequency ω_0. The possibility of solutions with two frequencies has been discussed in [34]. In this analysis, we will ignore the gain-compression terms. In the absence of gain anisotropy and feedback, solutions are written for the carrier densities and the field:

$$N_s^x = N_{\rm th} + \frac{2\gamma_a}{\Gamma G_N}, \quad N_s^y = N_{\rm th} - \frac{2\gamma_a}{\Gamma G_N}, \quad S_s = 0,$$

$$e_\pm^2 = \frac{P - N_s/\tau_e}{2\Gamma G_N(N_s - N_0)}$$

for the angle ψ and the difference frequency:

$$\varphi^x=0, \quad \Delta\omega_s^x=\omega_s^x-\omega_0=-\gamma_b+\alpha\gamma_a$$

for x-linear polarized light (first solution x),

$$\varphi^y=\pi/2, \quad \Delta\omega_s^y=\gamma_b-\alpha\gamma_a$$

for y-linear polarized light (second solution y). Two elliptical solutions could exist (see Appendix C).

In the following, we will analyze the stability of the linearly polarized modes with weak polarized feedback.

2. Linearly polarized solutions with polarized optical feedback

If the polarizer makes an angle θ with respect to the laser axes ($0°<\theta<90°$), then $c_+\neq c_-$ and $n_s\neq 0$, $e_+\neq e$. The stability of elliptical solutions should be studied. This last case is not trivial as one should find the phase condition from coupled nonlinear equations. Recall that in this study $m=m_+=m_-=\frac{1}{2}$ and $c_+=c_-=-\frac{1}{2}$ (or $\frac{1}{2}$) for the matrix elements in Eq. (6). The diagonal terms m modify the gain and the frequency of the stationary solutions and the cross terms c_+ affect the *anisotropy of the linearly polarized* modes. They can be taken away by introducing a new amplitude anisotropy:

$$\gamma_a'=\gamma_a-\frac{X}{\tau_c}\,c_+\,\cos(\omega_s\tau) \tag{7}$$

and a phase anisotropy

$$\gamma_b'=\gamma_b+\frac{X}{\tau_c}\,c_+\,\sin(\omega_s\tau), \tag{8}$$

where the stationary phase $\omega_s\tau$ may have different expressions $\omega_s^x\tau$, $\omega_s^y\tau$ for the x and y modes as shown in the following. These terms are now frequency dependent.

With this slight modification brought by polarized optical feedback, one can write the new stationary solutions for the two polarizations $x(\varphi^x=0)$ and $y(\varphi^y=\pi/2)$. The stationary *spin* carrier density S is equal to zero. The intensity has the same form as in the preceding section:

$$e_{\pm}^2=\frac{P-N_s/\tau_e}{2\Gamma G_N(N_s-N_0)}. \tag{9}$$

Two conditions will be obtained for the phase and the gain. The gain condition gives the value of the stationary carrier density N_s:

$$N_s^x=N_{\rm th}+\frac{2}{\Gamma G_N}\,\gamma_a, \tag{10}$$

$$N_s^y=N_{\rm th}-\frac{2}{\Gamma G_N}\left(\gamma_a+\frac{X}{\tau_c}\cos(\omega_s^y\tau)\right). \tag{11}$$

The phase condition is also written for each mode:

$$\Delta\omega_s^x\tau=\omega_s^x\tau-\omega_0\tau=-\gamma_b\tau+\alpha\gamma_a\tau, \tag{12}$$

$$\Delta\omega_s^y\tau=\omega_s^y\tau-\omega_0\tau$$
$$=\gamma_b\tau-\alpha\gamma_a\tau-X\,\frac{\tau}{\tau_c}\,\sqrt{1+\alpha^2}\,\sin[\omega_s^y\tau+A\,\tan(\alpha)]. \tag{13}$$

From Eqs. (10)–(13), one can see that only the gain and phase conditions on mode Y are affected because the optical feedback is applied to this mode.

Equation (13) is similar to the usual one obtained for conventional lasers with optical feedback [39]. Modes and antimodes are obtained. The frequency separation between two stationary solutions is $c/4L$ [39]. They are located on an ellipse along the gain versus frequency chart:

$$\left[\frac{\Delta G(X)}{2}\right]^2+\left[\Delta\omega(X)-\frac{\alpha}{2}\,\Delta G(X)\right]^2=\left(\frac{X}{\tau_c}\right)^2, \tag{14}$$

with $\Delta G(X)=\Gamma G_N(N_s-N_{\rm th})+2\gamma_a$, $\Delta\omega(X)=\omega_s-\omega_0-\gamma_b+\alpha\gamma_a$.

Only the solutions on the lower part of the ellipse, which are called modes, are stable [39]. They are separated by the free spectral range of the passive external cavity $c/2L$. In the case of an extended cavity with a quarter-wavelength plate (ECQW), one could observe Fabry-Pérot spectra with external-cavity modes separated by $c/4L$ [49]. As a matter of fact, the FSR between stable modes is always $c/2L$ in this case, but along new eigenaxes of the coupled cavity. The $c/4L$ range comes from the beating between two differently polarized combs of modes [49] as already demonstrated theoretically [50].

Equation (13) indicates that the frequency shifts when optical feedback is applied. This shift is extremely useful as it allows for the measurement of feedback strengths. The last term in Eq. (13) is responsible for this shift. Its amplitude is written $C:=X(\tau/\tau_c)\sqrt{1+\alpha^2}=54.6Lr_3$ when L is expressed in cm. It has been demonstrated [40] that only one external-cavity mode is the solution if $C=X(\tau/\tau_c)\sqrt{1+\alpha^2}=54.6L(\text{cm})r_3\leqslant 1$. The number of solutions of the phase Eq. (13), is given by value of C. For instance, to have one solution, if L is equal to 3 cm, r_3 has to be lower than 6.1×10^{-3}; if $L=15$ cm, $r_3<1.2\times10^{-3}$. One should keep in mind that a VCSEL has a very short cavity (a few micrometers long) with high reflectors [51] so that the feedback rate (proportional to the ratio ''power transmitivity'' over ''the laser-cavity length'') is usually the same as in conventional lasers (with lower reflectivities but with longer laser cavity).

It explains why the shorter the cavity is, the more stable the system is. In the POF case, if one wants to avoid instabilities due to feedback, one tries to get one or very few external-cavity modes, by controlling the feedback strength. One or three modes are obtained if $C\leqslant 4.6$ ($r_3=2.8\%$ if $L=3$ cm) [40]. This last condition has always been checked in the experiment. The linear stability analysis will be performed for $C<1$, a condition for which only a single external-cavity mode is stable.

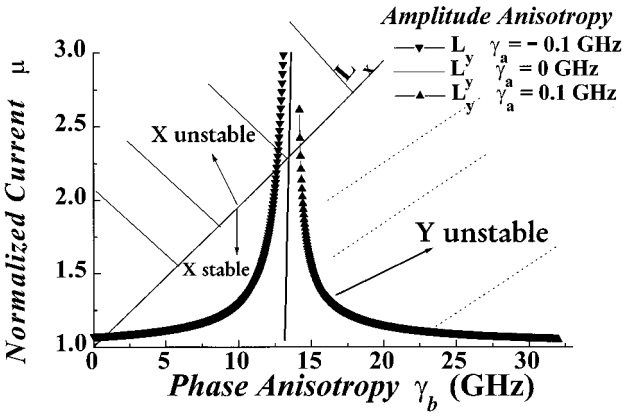

FIG. 5. Stability diagram for the x-polarized and y-polarized mode in the steady state approximation. The x-polarized mode is stable under the straight line which almost does not depend on the amplitude anisotropies (for low anisotropy $|\gamma_a|<0.4$ Ghz). The stability of the y-polarized mode is greatly dependent on the value of the amplitude anisotropy.

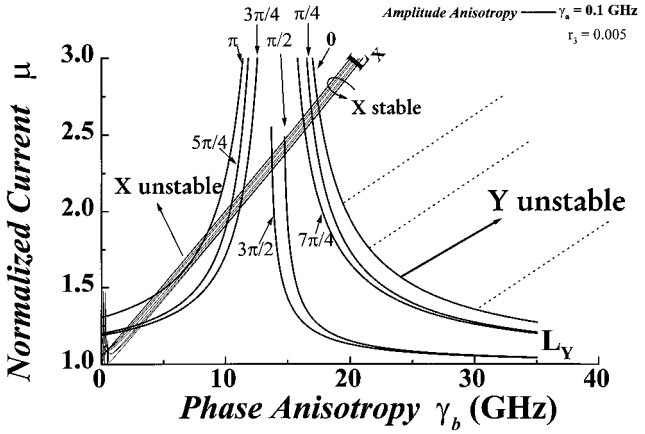

FIG. 6. Stability diagram with feedback for different values of the stationary phase $\omega_s^y\tau$ (from 0 to $7\pi/8$). When $\omega_s^y\tau=\pi/2, 3\pi/2$, the stability diagram is almost the same as in Fig. 5.

3. Linear stability analysis

A small complex perturbation $a_\pm(t)$ is applied to each stationary solution and the perturbed fields are written $E_\pm(t)=[e_\pm+a_\pm(t)]e^{i(\Delta\omega_s t\pm\varphi)}$. The perturbed variables are written, with Δ, δ, $N=N_s+\Delta$, $S=S_s+\delta$. The new linear system is decoupled into two sets of three equations (see Appendix E and [34]) and has solutions of the form $a_\pm(t)=a_{\pm 0}e^{\lambda t}$, $\Delta(t)=\Delta_0 e^{\lambda t}$, $\delta(t)=\delta_0 e^{\lambda t}$. A first set will give the stability of a polarized solution with respect to the same polarization. In this first set, the equation for the state without feedback (x for $\theta=0°$ or y for $0=90°$) gives a solution which is always stable (as it is similar to the equation for a single-frequency and monopolarized free-running laser). The other state is subject to optical feedback. Its stability depends on the feedback conditions. The equations are the same as those for scalar lasers with feedback and a similar analysis could be done. The conditions of our study are taken to be in the first feedback regime such that only one external-cavity mode is stable and able to oscillate ($C<1$). However, for relatively strong feedback, one has to keep in mind that the stability of different external-cavity modes should be analyzed. Within our conditions, the first set of equations is always stable. The stability is then determined by the second set which describes the interaction between orthogonal modes, due to optical feedback and spin relaxation coupling.

We first recall the stability analysis without feedback. The results are shown in Fig. 5 for three values of the amplitude anisotropy, in the normalized current (μ)-phase anisotropy (γ_b) chart as proposed by Martin-Regalado *et al.* [34]. The scale of the phase anisotropy is linear and the normalized current is defined as $\mu=P/P_{\rm th}$ with respect to the pump at threshold $P_{\rm th}=N_{\rm th}/\tau_e$.

Lines L_x and L_y in Fig. 5 border the stability region of the x and y modes: they are given (see Appendix) for the x-polarized mode by Lyapounov exponents which are real, and for the y-polarized mode by the real part of Lyapounov exponents which are complex conjugate. Setting the real part of these exponents to zero, the equations for L_x, L_y give the pump parameter P as a complex function of the laser ($\gamma_a,\gamma_b,\alpha,\ldots$) [and in our case of feedback parameters (X,τ)]. It is this function which allows us to draw the border between stable and unstable regions in Figs. 5 and 6.

We can divide this phase diagram into four regions. For example, at the left (right) of the L_y curve, mode y is stable (unstable). At the left (right) of the L_x curve, mode x is unstable (stable). One sees that for $\gamma_b=15$ GHz, both modes are stable if $\gamma_a=0.1$ GHz and $\mu<1.5$. For the same values, mode x is stable and mode y unstable if $\gamma_a\leqslant 0$. For higher values of the phase anisotropy $\gamma_b(>25$ GHz), only the mode x is stable.

When an optical feedback is applied along the Y axis of the laser, we obtain new expression for the border lines L_x, L_y.

For the x-polarized mode, P is given by

$$P=N_s^x+\frac{\tau_e}{\tau_s}\times\frac{(N_s^x-N_0)\left[\left(2\gamma_a+\frac{X}{\tau_c}\cos(\omega_s^x\tau)\right)^2+\left(2\gamma_b-\frac{X}{\tau_c}\sin(\omega_s^x\tau)\right)^2\right]}{\Gamma G_N(N_s^x-N_0)\left(2(\alpha\gamma_b+\gamma_a)+\frac{X}{\tau_c}[\cos(\omega_s^x\tau)-\alpha\sin(\omega_s^x\tau)]\right)-\left[\left(2\gamma_a+\frac{X}{\tau_c}\cos(\omega_s^x\tau)\right)^2+\left(2\gamma_b-\frac{X}{\tau_c}\sin(\omega_s^x\tau)\right)^2\right]},\tag{15}$$

with $N_s^x=N_{\rm th}+2\gamma_a/\Gamma G_N$, $\Delta\omega_s^x\tau=\omega_s^x\tau-\omega_0\tau=-\gamma_b\tau\Delta\omega_s^x\tau=\omega_s^x\tau-\omega_0\tau=-\gamma_b\tau+\alpha\gamma_a\tau$ [relations (10) and (12)].

For the y-polarized mode, P is given in a second-order polynomial expression:

$$\frac{\Gamma G_N}{\tau_c}(N_s^y-N_0)y\left(\frac{1}{\tau_s}+\frac{y}{\tau_c}+2(\gamma_a-\alpha\gamma_b)+\frac{X}{\tau_c}[\cos(\omega_s^y\tau)+\alpha\,\sin(\omega_s^y\tau)]\right)+2\left(\frac{1}{\tau_s}+\frac{y}{\tau_c}\right)\left(2\gamma_a+\frac{X}{\tau_c}\cos(\omega_s^y\tau)\right)$$
$$\times\left[\frac{1}{\tau_s}+\frac{y}{\tau_c}+2\left(2\gamma_a+\frac{X}{\tau_c}\cos(\omega_s^y\tau)\right)\right]+2\left[\left(2\gamma_a+\frac{X}{\tau_c}\cos(\omega_s^y\tau)\right)^2+\left(-2\gamma_b+\frac{X}{\tau_c}\sin(\omega_s^y\tau)\right)^2\right]$$
$$\times\left(2\gamma_a+\frac{X}{\tau_c}\cos(\omega_s^y\tau)\right)=0, \tag{16}$$

with $y=(P-N_s^y)/(N_s^y-N_0)$ and relations (11) and (13).

Expressions (15) and (16) enable us to draw L_x, L_y in different charts ($\mu-\gamma_b$, $\mu-\omega_s\tau$, $\mu-\omega_0\tau$ or $r_3-\omega_0\tau$) as one has to find roots of a polynomial of order varying from 1 to 3 (3 if X is the variable). These separatrixes are frequency dependent and will change with the phase of the feedback light. In the first example, we will take $\gamma_a=0.1$ GHz, $\gamma_b=15$ GHz or higher. Without feedback, the amplitude anisotropy will yield a gain difference at threshold for modes x and y, which is $4\gamma_a/\Gamma G_N$ ($=0.073\%N_{\rm th}$ if $\gamma_a=0.1$ GHz).

In the second example, we will take a stronger amplitude anisotropy $\gamma_a=-4$ GHz and weak phase anisotropy $\gamma_b=0.2$ GHz.

When optical feedback is applied, both phase and amplitude anisotropies are modified, leading to a change in the stability diagram given in Fig. 5.

(1) Weak amplitude anisotropies. This study is devoted to the influence of the spin interaction on polarization properties of VCSELs under external feedback at line center, for weak amplitude anisotropies.

The amplitude anisotropy γ_a, as long as it remains small (<1 GHz), has mainly an influence on the stability of the mode y (Fig. 5). When it is equal to zero, L_y is almost a vertical straight line (at $\gamma_b=1/2\alpha\tau_s$, see Appendix E). For positive amplitude anisotropy, bistable operation could exist for low current. But if the amplitude anisotropy is taken as positive and small, one can consider that only one mode is stable for high birefringence (>25 GHz).

We can give many representations of the effect of polarized feedback on the stability of each polarized mode. We will first focus on the influence of the external phase. Figure 6 sums up the influence of optical feedback in the same parameter representation $\mu-\gamma_b$ as in Fig. 5. The stationary phase $\phi_s=\omega_s^y\tau$ which is related to the phase $\psi=\omega_0\tau$ of the external feedback light, will change the stability of the polarized modes, as shown for $r_3=0.005$, $\gamma_a=0.1$ GHz. Several curves for L_x and L_y are drawn in Fig. 6 for $\phi_s=\omega_s^y\tau=n\pi/4$ with $0\leqslant n\leqslant 7$. Curves labeled L_y are very well separated, showing a strong influence of the phase on the stability of y modes. Curves labeled L_x remain straight lines with a small shift. The effect of feedback is similar to the effect of the amplitude anisotropy so that the stability of the x-polarized mode is slightly affected. This effect can be understood if, as outlined in the following, the feedback effect is taken proportional to $\cos(\omega_s\tau)$. When $\omega_s\tau=\pi/2, 3\pi/2$, this factor is equal to zero and the lines are close to those obtained without feedback (compare with the L_y line obtained without feedback for $\gamma_a=0.1$ GHz in Fig. 5). For $\omega_s\tau=0$, $7\pi/4$, and $\pi/4$, and $\cos(\omega_s\tau)$ is positive and the effect of POF will be equivalent to a greater internal amplitude anisotropy. For $\omega_s\tau=3\pi/4$, $5\pi/4$, and π, $\cos(\omega_s\tau)$ is negative and the total effect of amplitude anisotropy and POF will be similar to a case where the amplitude anisotropy γ_a is negative (see the L_y line obtained for $\gamma_a=-0.1$ GHz in Fig. 5). Similar diagrams have been obtained for negative amplitude anisotropy. Thus when the stationary phase is modulated, the stability lines will move according to the representation given in Fig. 6.

It is then convenient to give the stability diagram in the chart normalized current-stationary phase as shown in Fig. 7 for different values of the phase anisotropy. Mode y is unstable between two lines which are symmetric to each other around π. In other words, as the system is periodic and symmetric with the stationary phase (equations for the stability contain only expressions of the form $e^{i\phi s}$), the calculations could be limited to values of the phase between 0 and π. The full chart is obtained by mirroring the restricted diagram with respect to the line $\omega_s\tau=\pi$. If the phase anisotropy is increased, the domain of stability of mode y in the chart $\mu-\omega_s\tau$ will shrink as the operating point moves away from the modulated L_y line (as can be seen in Fig. 6). For comparison, curves are drawn for $\gamma_b=15$ GHz and $\gamma_b=30$ GHz

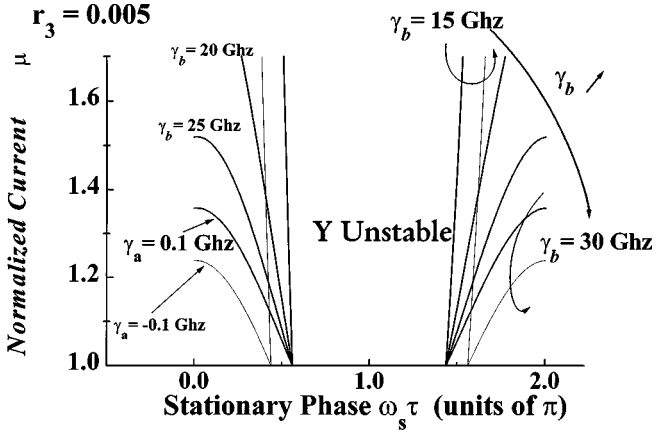

FIG. 7. Stability diagram with feedback in the phase-bias current chart for different values of the birefringence and of the amplitude anisotropy ($\gamma_a=0.1$ GHz; $\gamma_a=-0.1$ GHz). $r_3=0.5\%$.

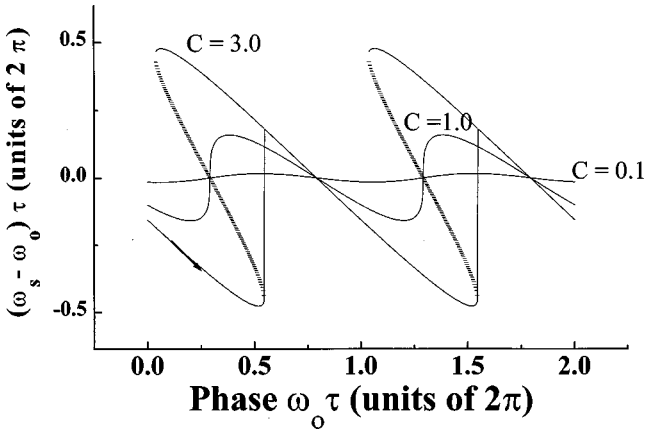

FIG. 8. Stationary phase versus external-cavity phase for three values of C.

with $\gamma_a = -0.1$ GHz. For instance, if we look at the two sets of curves for $\gamma_b = 15$ GHz, the stability domain of mode y is smaller when $\gamma_a = -0.1$ GHz than when $\gamma_a = 0.1$ GHz. Considering the case without feedback in Fig. 5 and fixing an operating point at 25 GHz, 1.5 in this chart show that this operating point is closer from the stability line when the amplitude anisotropy is positive, so that when the optical feedback is applied, the excursion for the phase has to be shorter to reach the stable region.

In summary, Fig. 7 shows the stability diagram drawn in the plane $(\mu, \omega_s \tau)$. However, in the experiment, the control parameter is the phase of the external-cavity field $\psi = \omega_0 \tau$ and not $\omega_s \tau$. Stability diagrams can be easily sketched in the plane $(\mu, \omega_0 \tau)$ because the stationary phase $\omega_s \tau$ is a function of the phase $\omega_0 \tau$ of the external-cavity field, as a solution of the transcendental equation (13). Figure 8 gives a classical representation of $\omega_s^y \tau - \omega_0 \tau$ versus $\omega_0 \tau$. $\omega_s^y \tau - \omega_0 \tau$ remains single valued as long as the feedback strength is weak $(C < 1)$. For higher values, the stationary phase could be multivalued. In any case, the stationary phase is a nonlinear function of the phase of the external-cavity field. $\omega_0 \tau = \pi$ is no longer a mirror point and as shown in Fig. 9, the dependency on the external phase $\omega_0 \tau$ will break the symmetry around $\omega_0 \tau = \pi$. In Fig. 9(a), the scale for normalized current has been enlarged in order to see the curve separating the stability regions of the x-polarized mode. It is almost a straight horizontal line at $\mu = 2.4$. Under this line mode x is stable. Other curves crossing the phase axis in Fig. 9(a) and all curves in Figs. 9(b)–9(d) are stability lines for

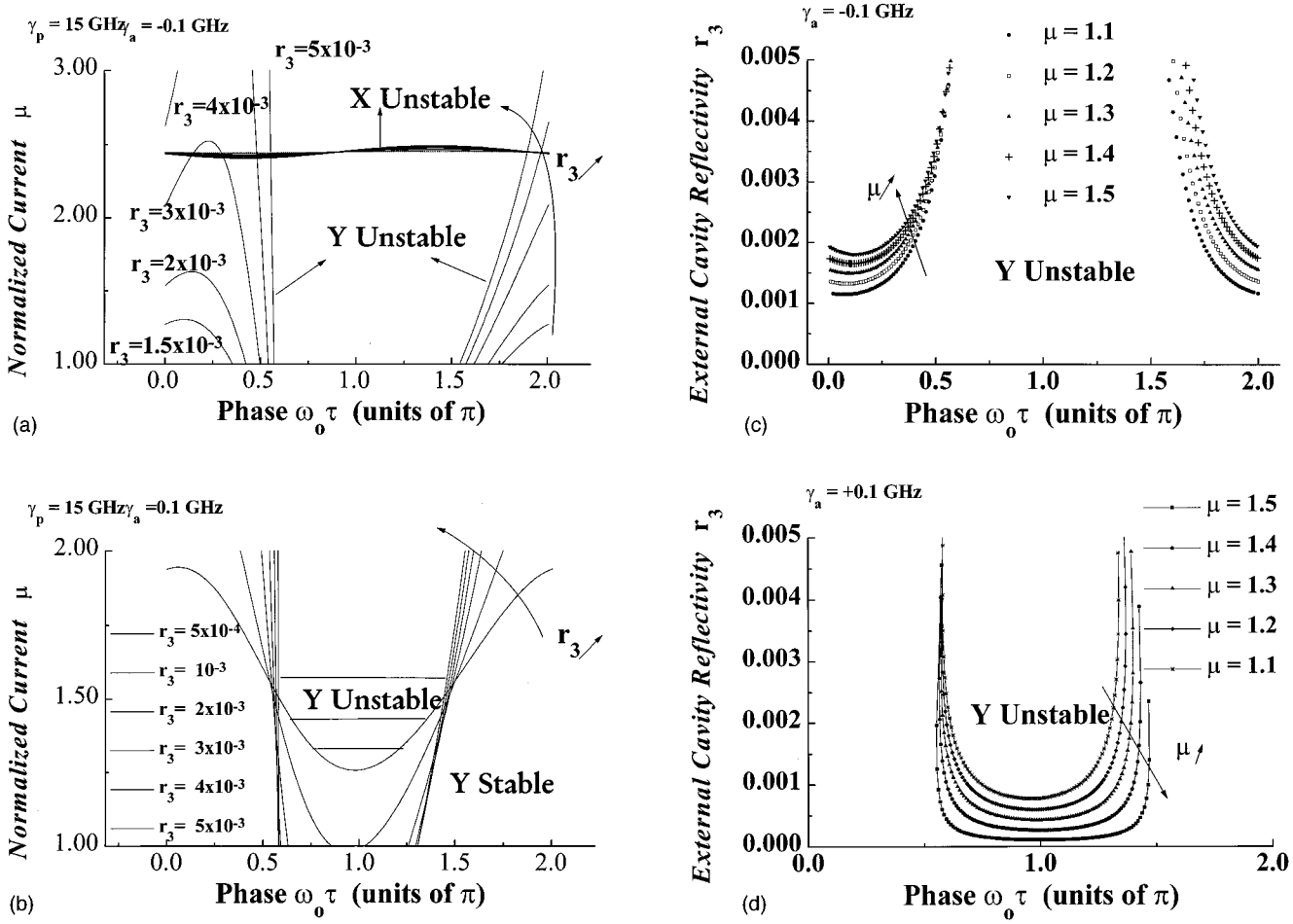

FIG. 9. Stability diagram with feedback in the optical phase-bias current chart: (a) for different values of r_3 with $\gamma_a = -0.1$ Ghz, $\gamma_b = 15$ Ghz, $\mu = 1.3$. (b) For different values of $r_3 = 0.1$ Ghz, $\gamma_b = 15$ Ghz, $\mu = 1.3$. In the phase-external reflectivity chart: (c) for different values of the bias current with $\gamma_a = -0.1$ Ghz, $\gamma_b = 15$ Ghz. (d) For different values of the bias current with $\gamma_a = 0.1$ Ghz, $\gamma_b = 15$ Ghz.

mode y. Then the x-polarized mode always remains stable for the experimental range of μ (<1.8). Note that in Fig. 7, the L_x curve is not seen as it is located at higher values of the normalized current.

Figures 9(a) and 9(b) show for several values of the feedback strength r_3 the lines separating the stability region of mode y. The feedback strength should be high enough to be able to change the stability of mode y. For high r_3, the stability lines L_y are almost straight lines located at $\pi/2$, $3\pi/2$. In this case, the exact positions are dependent only on the amplitude anisotropy. One should stress the very different stability diagram when the sign of the amplitude anisotropy is changed [compare Figs. 9(a) and 9(b)]. Then the mode y is stable for low values of the bias current as expected (Fig. 5, $\gamma_b=15$ GHz, $\gamma_a=0.1$ GHz). In Figs. 9(c) and 9(d), the lines separating the y-stability regions are drawn in the plane (external-cavity reflectivity r_3, phase of the external-cavity field $\omega_0\tau$). When the amplitude anisotropy is positive (negative) and if the bias current is increased, the external reflectivity at which the mode y becomes stable decreased (increased). This property gives an easy way to characterize the sign of the amplitude anisotropy.

For stronger feedback regimes ($C>1$), the switching is dependent on the initial mode and bistable behavior between external-cavity modes could be observed [52] as outlined in the next section and observed in the experiment.

We may question whether the stability is mainly influenced by gain effects or dispersion properties of the material. Taking Henry's coefficient α equal to zero will have a tendency to severely shrink the unstable domain of the y-polarized mode as in this case both modes are stable for the bare cavity. We mentioned that optical feedback could be taken into account by considering new birefringence and amplitude anisotropy [relations (7) and (8)]. If we consider that the birefringence is not influenced by optical feedback and if we set $\gamma_p'=\gamma_p$ in all the characteristic equations, all results presented up to now will remain essentially the same. In order words, the stability of mode y is mostly affected by the amplitude anisotropy. This could be understood as the contribution due to feedback X/τ_c is of the order of 0.25 GHz when $r_3=10^{-3}$ and is of the same order as the internal amplitude anisotropy. Changing the external-cavity phase will change the external-cavity anisotropy, then the total amplitude anisotropy, and it will greatly alter the L_y line. This is why in this first example, optical feedback has mainly an influence on amplitude anisotropy and then on threshold. Both quantities are related to the gain. The difference between losses of the two polarized modes is $4\gamma_a$ and should be compensated for by the frequency-dependent losses $\gamma_f=2r_3\cos(\omega_s\tau)$, which are introduced by optical feedback. The sign of γ_f is inverted when the phase of the feedback light moves from $\pi/2$ to $3\pi/2$. Then, mode y could become stable. This interpretation is confirmed by Figs. 7 and 9. Recall that with $\gamma_a>0$, the mode y has lower losses [relations (10) and (11)] so that it will be easier to make it stable as described by Fig. 5. In fact, the main features of the results could be interpreted by the following simple image: the stronger mode will survive, the weaker mode will die. Nevertheless recall that in this analysis, the stability of the mode y is influenced by the interaction with the mode x through the parameter S.

However, for lower values of the birefringence γ_b and strong amplitude anisotropy γ_a, the stability of the x-polarized mode changes. This is discussed in the next paragraph.

(2) Strong amplitude anisotropies. In this paragraph we will discuss the influence of a high amplitude anisotropy γ_a (>1 GHz) on the stability properties. Change of stability could be observed for γ_a equal to a few-GHz and $\gamma_b=36$ GHz. In this case one has to increase the value of the external-mirror reflectivity r_3 to a few percent to compensate for the higher value of the amplitude anisotropy. The analysis remains correct as long as the feedback is weak ($C<1$). If the birefringence is low (<1 GHz) and γ_a equal to a few-GHz, it is possible to change the stability of both modes when the effective reflectivity is increased to a few percent (for instance: $\gamma_a=-3.1$ GHz and $\gamma_b=0.1$ GHz; $r_3=0.03$). Results given by Eq. (8) indicate that in this case, the system could cross the stability line $\gamma_b=0$ GHz. Then the stability of x and y modes is interchanged. Note that in this case, the stability for y ($\gamma_a\ll 0$) could be given by real Lyapounov exponents.

D. Numerical results

We used standard algorithm (Gear) to integrate the system of Eqs. (1), (2), and (6) with noise. In order to ensure a temporal Gaussian distribution of the spontaneous field, a time step of 10 ps was taken. The gain-compression coefficients $\beta_\pm, \theta_\pm$ in Eq. (6) are needed to describe the experiment. When these terms are omitted, the signal becomes extremely noisy when there is a polarization switching. We took $\beta_+=\beta_-=\theta_+=\theta_-=10^{-23}\,\mathrm{m}^{-3}$. The values of self- and cross-gain-compression coefficients are not important in the case of external cavity with quarter-wavelength plate [49] as the feedback strength is strong, while they will favor or annihilate the modulation of the polarization state in the POF case. It is not surprising that those parameters could even have an effect on the stability of the polarized modes [53]. Further investigations will be necessary to know what the influence of $\beta_+, \theta_{+,\ldots}$ (see Appendix C) really is and to discriminate the role of the spin-interaction variable S from the one of the gain-compression terms. In all the simulations, the external-cavity phase is directly modulated (at f_ϕ). When the external-cavity length is varied over a wavelength, the round-trip time and other parameters remain unchanged. On the other hand, when the laser frequency is changed by direct current modulation, some parameters such as the differential gain could also be modulated. However, the modulation depth is so weak in the experiment (-20.5 dBm at 1 MHz) that all parameters may also be considered constant, including the bias current, which is fixed at 1.3.

No polarization switching is obtained without noise terms. This could be the signature of the bistable behavior. When there is no spontaneous emission, the system stabilizes either the x-polarized mode or the y-polarized mode after a transient period. With noise, the two modes are in permanent competition and the system is able to switch to another mode. Switching is obtained for positive and negative amplitude anisotropy. However, switching disappears for $\gamma_b>25$ GHz with $\gamma_a=-0.1$ GHz, and for $\gamma_b>35$ GHz with $\gamma_a=0.1$ GHz. Figure 10(a) describes the polarization-state

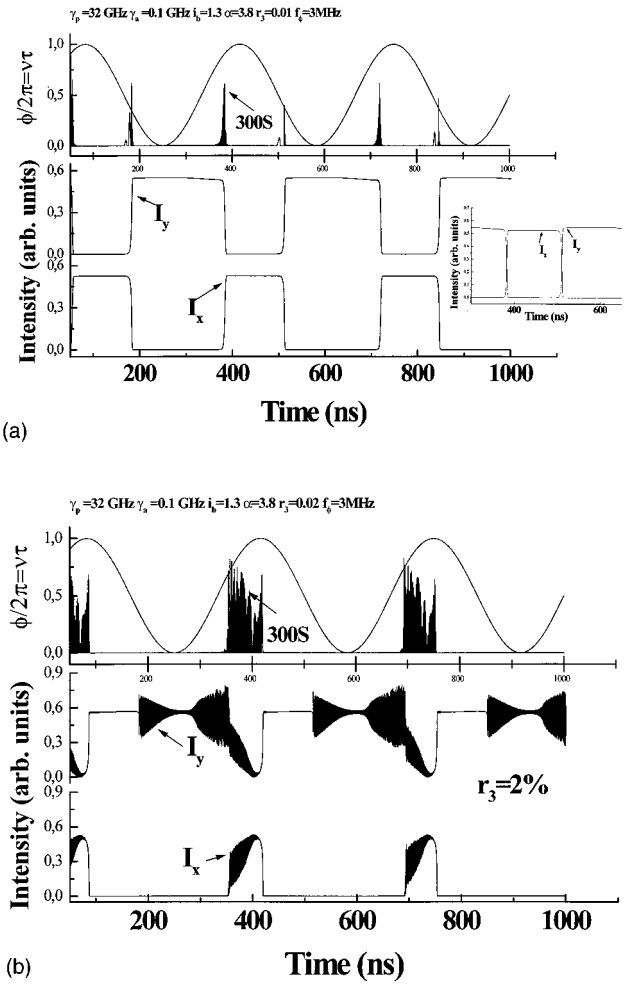

FIG. 10. Simulation of polarization switchings. Upper graph represents the modulation of the phase at 3 MHz and 300 times the variation of the normalized carrier difference between the spin levels. It is no longer equal to zero when the laser changes its polarization. $\gamma_p = 32$ GHz, $\gamma_a = 0.1$ GHz, $\mu = 1.3$, and (a) $r_3 = 1\%$, (b) $r_3 = 2\%$. In this last case, several external-cavity modes could exist depending on the value of the phase. This trend could explain the noisy trace (see text).

control with $\gamma_a = 0.1$ GHz, $\gamma_b = 32$ GHz, $f_\phi = 3$ MHz, $\tau = 500$ ps ($L = 5$ cm), $r_3 = 1\%$. In the inset, one sees that the intensity of the mode with optical feedback (y) is slightly amplified in comparison to the output of mode x. In agreement with the linear stability analysis (LSA), no control of the polarization is obtained for too low values of the feedback strength. Similar results were obtained for shorter cavity lengths and different values of the anisotropies.

Figure 10(b) illustrates the situation for higher feedback strength ($r_3 = 2\%$, $C = 3.27$) where the transition becomes noisy. In Fig. 10(a), only one external-cavity mode will operate while in Fig. 10(b), three external-cavity modes will exist [49], generating partition noise which will disturb the phase. Another question is to know whether the standard equations (without inclusion of spin interaction) will give correct results. When the carrier difference between spin levels is removed, identical results are obtained (the results were also obtained for POF and extended cavity with quarter-wavelength plate by setting $S = 0$). At this point, the precise role of the carrier difference between spin levels and whether it is important or not is not yet clear. In Figs. 10(a) and 10(b), the normalized coupling parameter ($\times 300$) between spin levels S has been sketched, in order to show that the spin relaxation is not equal to zero during the polarization switch.

IV. CONCLUSION

We have described the main effects of inserting a polarizer in a VCSEL-extended cavity. The control of the internal anisotropy with an external anisotropy enables us to command the polarization state of a VCSEL. The control parameter is the phase of the external cavity field. It can be varied with the external cavity length or the laser frequency. The chirp effect can be used up to 50 MHz, due to large thermal effects. For higher frequencies, thermal following is not adiabatic and modulation depths should be increased. Transverse modes are excited and partition noise makes the switching erratic. One could imagine reaching very high modulation frequencies by modulating the external phase using electro-optical components based on Kerr or Pockels effects or by modulating the feedback strength by electro absorption (via Stark effects in multiple quantum wells).

Polarization control with polarized feedback is complex to analyze. We have limited our study to the particular situation where the laser emits at line center. The linear stability analysis shows that the stability of the y-polarized mode is greatly affected when the bare cavity is coupled to an external cavity. In fact, a free laser which is monostable (with one mode and one polarization) could become bistable in polarization when polarized optical feedback is applied. However, numerical studies show that the insertion of noise and gain-compression coefficients is necessary to describe the experimentally observed polarization switching. The primary role of noise is to induce the flip onto the mode with lower losses. This feature is by far different from the situation encountered in He-Ne lasers [27].

Future studies will be necessary to clarify the respective influence of gain-compression coefficients and spin relaxation. As one could generate switching when modulating the optical frequency through chirp in the thermal band, this setup could give future prospects to measure and theoretically characterize the dynamical influence of temperature [54].

ACKNOWLEDGMENTS

We acknowledge the careful reading of Dr. B. Meziane and the financial support of France Telecom through Contract Number 93 1B140.

APPENDIX A: INSERTION OF THE CARRIER DENSITY AT TRANSPARENCY

Standard analysis [55] (semiclassical analysis, adiabatic elimination of the polarization, rotating-wave approximation) yields the following set for the fields $\mathcal{E}_\pm$ ($\mathcal{I}_\pm$ the intensities) and the variables n, s:

$$\frac{\partial n}{\partial t}=\Lambda-\gamma_{\parallel}n-\frac{1}{2\hbar}\mathscr{l}(1-\xi_{--}\mathcal{I}_{-}-\xi_{-+}\mathcal{I}_{+})(n-s-1)\mathcal{I}_{-}$$

$$-\frac{1}{2\hbar}\mathscr{l}(1-\xi_{++}\mathcal{I}_{+}-\xi_{+-}\mathcal{I}_{-})(n+s-1)\mathcal{I}_{+},$$

$$\frac{\partial s}{\partial t}=-\gamma_{\parallel}s-2\gamma_{s}s+\frac{1}{2\hbar}\mathscr{l}(1-\xi_{--}\mathcal{I}_{-}-\xi_{-+}\mathcal{I}_{+})(n-s$$

$$-1)\mathcal{I}_{-}-\frac{1}{2\hbar}\mathscr{l}(1-\xi_{++}\mathcal{I}_{+}-\xi_{+-}\mathcal{I}_{-})(n+s-1)\mathcal{I}_{+},$$

$$\dot{\mathcal{E}}_{\pm}=-\frac{\mathcal{E}_{\pm}}{2\tau_{p}}-i(\Omega_{\pm}-\omega_{\pm})\mathcal{E}_{\pm}+\frac{\omega_{\pm}}{2\varepsilon}\mathscr{l}(1-\xi_{\pm\pm}\mathcal{I}_{\pm}-\xi_{\pm\mp}\mathcal{I}_{\mp}$$

$$-i\alpha)(n\pm s-1)\mathcal{E}_{\pm},$$

where

$$\gamma_{\parallel}=\frac{1}{\tau_{e}},\quad n=\frac{1}{2}(n_{1}+n_{-1}+n_{3}+n_{-3}),$$

$$s=\frac{1}{2}(-n_{1}-n_{3}+n_{-1}+n_{-3}),\quad \mathcal{I}_{\pm}=|\mathcal{E}_{\pm}|^{2},$$

$$\mathscr{l}=\frac{1}{\hbar}|\mu_{hh}|^{2}\frac{\gamma_{\perp}}{\gamma_{\perp}^{2}+(\omega_{\pm}-\omega_{cv})^{2}},$$

$$\gamma_{\perp}=\frac{1}{2}(\gamma_{e}+\gamma_{h})\approx 10-20\ \mathrm{ps}^{-1}$$

is the relaxation time for the polarization (coherent term for the dipoles). $\omega_{cv}=(E_{c}-E_{v})/\hbar$ is the frequency associated with the energy transition. μ_{hh} is the dipole element between the conduction and the valence band. $n_{1}=\rho_{11}$ is the density of electrons with $J_{z}=\frac{1}{2}$, $n_{-1}=\rho_{-1-1}$ the density of electrons with $J_{z}=-\frac{1}{2}$, $n_{3}=1-\rho_{33}$ the density of holes with $J_{z}=\frac{3}{2}$, $n_{-3}=1-\rho_{-3-3}$ the density of holes with $J_{z}=-\frac{3}{2}$. $\rho_{ij\ \{ij=1,-3,1,3\}}$ is the generic density matrix element. α is the phase-coupling parameter. Λ is the pump parameter. $\xi_{-+,\ldots}$ are the gain-compression parameters. ω is the optical angular frequency and $\omega_{\pm}=\omega$. Here we have $\Omega_{\pm}=\omega_{t}$. Summing over the electron momentum gives the macroscopic variables:

$$P=\eta\frac{J}{ed}=\frac{1}{V}\sum_{\mathbf{k}}\Lambda$$

($\Lambda=\Lambda_{e}+\Lambda_{h}=\eta V\,J/ed$, η is the quantum efficiency, V is the volume of the active zone, d the thickness of the active zone),

$$N=\frac{1}{2V}\sum_{\mathbf{k}}(n_{1,\vec{\mathbf{k}}}+n_{-1,\vec{\mathbf{k}}}+n_{3,\vec{\mathbf{k}}}+n_{-3,\vec{\mathbf{k}}}),$$

$$S=\frac{1}{2V}\sum_{\mathbf{k}}(-\mathbf{n}_{\mathbf{1},\vec{\mathbf{k}}}-n_{3,\vec{\mathbf{k}}}+n_{-1,\vec{\mathbf{k}}}+n_{-3,\vec{\mathbf{k}}}),$$

and the carrier density at transparency $N_{0}=(1/2V)\Sigma_{\vec{\mathbf{k}}}1$. We assume that the gain depends linearly on the carrier density:

$$\frac{1}{2}\Gamma G_{N}(N\pm S-N_{0})\mathcal{E}_{\pm}=\frac{1}{2V}\sum_{\mathbf{k}}\frac{\omega_{\pm}}{2\varepsilon}\mathscr{l}_{\vec{\mathbf{k}}}(n_{\vec{\mathbf{k}}}+s_{\vec{\mathbf{k}}}-1)\mathcal{E}_{\pm}.$$

The optical field $\sqrt{\varepsilon/2\hbar\omega_{\pm}}\mathcal{E}_{\pm}^{*}$ is written $E_{\pm}$. The photon density $|E_{\pm}|^{2}$ is given by $I_{\pm}=\varepsilon\mathcal{I}_{\pm}/2\hbar\omega_{\pm}$ where ε is the permittivity.

APPENDIX B: NORMALIZED EQUATIONS AND SIMPLIFIED MODEL

If we normalize $N/N_{\mathrm{th}}\rightarrow N$, $S/N_{\mathrm{th}}\rightarrow n$, $|e_{\pm}|^{2}=(\tau_{e}/N_{\mathrm{th}}\tau_{p})I_{\pm}$, $t/\tau_{p}\rightarrow t$, $\mu=\tau_{e}P/N_{\mathrm{th}}$, and $\mathbf{b}=\tau_{p}\mathbf{M}$ and if we set $b=X\tau_{p}/\tau_{c}=0.69r_{3}$, $\gamma_{b}\tau_{p}\rightarrow\gamma_{b}$, $\xi_{e}=\tau_{p}/\tau_{e}=3.3\times10^{-3}$, $\xi_{s}=\tau_{p}/\tau_{s}=0.33$, $g=\Gamma G_{N}N_{\mathrm{th}}\tau_{p}=1.85$, $\eta=1-1/g=N_{0}/N_{\mathrm{th}}=0.46$, $\beta_{\pm}(\theta_{\pm})\rightarrow(N_{\mathrm{th}}\tau_{p}/\tau_{e})\beta_{\pm}(\theta_{\pm})$, we get from Eqs. (1)–(3)

$$\frac{dN}{dt}=\xi_{e}[\mu-N-g(1-\beta_{-}s_{-}-\theta_{-}s_{+})(N-n-\eta)s_{-}$$

$$-g(1-\beta_{+}s_{+}-\theta_{+}s_{-})(N+n-\eta)s_{+}],\tag{B1}$$

$$\frac{dn}{dt}=-\xi_{s}n+g\xi_{c}[(1-\beta_{-}s_{-}-\theta_{-}s_{+})(N-n-\eta)s_{-}$$

$$-(1-\beta_{+}s_{+}-\theta_{+}s_{-})(N+n-\eta)s_{+}],\tag{B2}$$

$$\dot{e}_{\pm}=-(\gamma_{a}+i\gamma_{b})e_{\mp}+\frac{1}{2}g(1+i\alpha)(N\pm n-1)e_{\pm}$$

$$-\frac{1}{2}g(\beta_{\pm}s_{\pm}+\theta_{\pm}s_{\mp})(N\pm n-\eta)e_{\pm}$$

$$+b_{\pm\pm}s_{\pm}(t-\tau)e^{-i\omega\tau}+b_{\pm\mp}s_{\mp}(t-\tau)e^{-i\omega\tau}.\tag{B3}$$

This system was used in the linear stability analysis and the numerical studies. This normalized set is equivalent to the one of Refs. [31, 34] when N_{0} is set equal to 0 and when the gain-compression terms are removed and with $\gamma=(1/\tau_{e})P=\gamma\mu$, $1/2\tau_{p}=\frac{1}{2}\Gamma G_{N}\rightarrow\kappa$,

$$S\rightarrow n,\quad \sqrt{\gamma/2\kappa}e_{\pm}=E_{\pm}:$$

$$\frac{dN}{dt}=-\gamma(N-\mu)-\gamma(N-n)|e_{-}|^{2}-\gamma(N+n)|e_{+}|^{2},$$

$$\frac{dn}{dt}=-\gamma_{s}n+\gamma(N-n)|e_{-}|^{2}-\gamma(N+n)|e_{+}|^{2},$$

$$\dot{e}_{\pm}=-\kappa e_{\pm}-i\omega_{0}e_{\pm}-(\gamma_{a}+i\gamma_{b})e_{\mp}+\kappa(1+i\alpha)(N\pm n)e_{\pm}.$$

APPENDIX C: EXPRESSIONS OF THE ELLIPTICAL SOLUTIONS

Two elliptical solutions are characterized by the following stationary values of the dynamical variables when the amplitude anisotropy is not considered: the intensities of the field components:

$$e_{\pm}^2=\frac{1}{2\Gamma G_N}\frac{(P-N_s/\tau_e\mp S_s/\tau_s)}{(N_s\pm S_s-N_0)}$$

$$=\frac{1}{2\Gamma G_N}\frac{(P-N_s/\tau_e)}{(N_{\rm th}-N_0)}\left(1\pm\frac{N_s-N_{\rm th}}{S_s}\right),$$

the spin-carrier density:

$$S_s^2=\frac{(N_s-N_{\rm th})(N_s-N_0)(P-N_s/\tau_e)}{[(N_{\rm th}-N_0)/\tau_s+P-N_s/\tau_c]},$$

the azimuth of the ellipse:

$$\tan(2\varphi)=\frac{1}{\alpha}\frac{N_s-N_{\rm th}}{S_s},$$

and the frequency difference:

$$\Delta\omega_s=\alpha\Gamma G_N\frac{(N_s-N_{\rm th})^2-S_s^2}{2(N_s-N_{\rm th})}$$

$$=\frac{(N_{\rm th}-N_0)[(N_s-N_{\rm th})/\tau_s-(P-N_s/\tau_e)]}{\tau_p N_{\rm th}[(N_{\rm th}-N_0)/\tau_s+(P-N_s/\tau_e)]}.$$

The value of N_s is one solution of the third-order equation

$$\gamma_b^2\left[\left(P-\frac{N_s}{\tau_e}\right)+\frac{(N_{\rm th}-N_0)}{\tau_s}\right]^2$$

$$=\left(\frac{\Gamma G_N\tau_p}{2}\right)^2(N_{\rm th}-N_0)\left[\left(P-\frac{N_s}{\tau_e}\right)-\frac{(N_s-N_{\rm th})}{\tau_s}\right]$$

$$\times\left\{\left[(N_s-N_{\rm th})\left(P-\frac{N_s}{\tau_e}\right)+\frac{(N_{\rm th}-N_0)}{\tau_s}\right]\right.$$

$$\left.\alpha^2\left(P-\frac{N_s}{\tau_e}\right)(N_s-N_0)\right\}.$$

The elliptical case is left to a future numerical study.

APPENDIX D: EQUATIONS FOR THE STATIONARY SOLUTIONS

The intensities are given by

$$(1-\beta_{\pm}e_{\pm}^2-\theta_{\pm}e_{\mp}^2)e_{\pm}^2=\frac{1}{2\Gamma G_N}\frac{(P-N_s/\tau_e\mp S_s/\tau_d)}{(N_s\pm S_s-N_0)}.$$

$e_{\pm}$ is the solution of a fourth-order equation. For $(e_+,e_-)\neq(0,0)$, the stationary quantities N_s, S_s, $\omega_s\tau,\psi$ are given by

$$\begin{pmatrix} \frac{1}{2}(1+i\alpha)\Gamma G_N(N_s-N_{\rm th}+S_s)+m_+\exp(-i\omega_s\tau)-i\Delta\omega_s & [-(\gamma_a+i\gamma_b)+c_+\exp(-i\omega_s\tau)]\exp(-i2\psi) \\ [-(\gamma_a+i\gamma_b)+c_-\exp(-i\omega_s\tau)]\exp(i2\psi) & \frac{1}{2}(1+i\alpha)\Gamma G_N(N_s-N_{\rm th}-S_s)+m_-\exp(-i\omega_s\tau)-i\Delta\omega_s \end{pmatrix}$$

$$\times\begin{pmatrix}e_+\\e_-\end{pmatrix}-\tfrac{1}{2}\Gamma G_N\begin{pmatrix}(N_s+S_s-N_0) & 0\\ 0 & (N_s-S_s-N_0)\end{pmatrix}\begin{pmatrix}e_+\\e_-\end{pmatrix}+\tfrac{1}{4}\begin{pmatrix}\dfrac{(P-N_s/\tau_e-S_s/\tau_s)}{e_+^2} & 0\\ 0 & \dfrac{(P-N_s/\tau_e+S_s/\tau_s)}{e_-^2}\end{pmatrix}\begin{pmatrix}e_+\\e_-\end{pmatrix}=0.$$

The imaginary part of the determinant of this matrix gives $\Delta\omega_s$ or the phase condition. The first equation gives $\tan(2\psi)$.

In this paper, the gain-compression terms are ignored.

APPENDIX E: LSA AND CRITICAL VALUES OF THE PUMP PARAMETER IN THE STABILITY DIAGRAM

A small complex perturbation $a_{\pm}(t)$ is applied to each stationary solution and the perturbed fields are written $E_{\pm}(t)=[e_{\pm}+a_{\pm}(t)]e^{i(\Delta\omega_s t\pm\varphi)}$. The perturbed variables are written with Δ, δ: $N=N_s+\Delta$, $S=S_s+\delta$. For the linearly polarized solutions x,y, two systems, which are decoupled, are obtained with

$$A=a_++a_-,\quad R=a_+-a_-,\quad \vec{\delta}_A=\begin{pmatrix}A\\A^*\\\Delta\end{pmatrix},\quad \vec{\delta}_R=\begin{pmatrix}R\\R^*\\\delta\end{pmatrix}$$

and using the Jacobian matrix

$$\frac{d\vec{\delta}_{A_y^x}}{dt}=\begin{pmatrix}0&0&c_1\\0&0&c_1^*\\-j_0&-j_0&-j_1\end{pmatrix}\vec{\delta}_A+f_y^x\begin{pmatrix}e^{-i\omega_s\tau}&0&0\\0&e^{i\omega_s\tau}&0\\0&0&0\end{pmatrix}$$

$$\times[\vec{\delta}_A(t-\tau)-\vec{\delta}_A],$$

$$\frac{d\vec{\delta}_{R_y^x}}{dt}=\begin{pmatrix}c_2&0&c_1\\0&c_2^*&c_1^*\\-j_0&-j_0&-j_2\end{pmatrix}\vec{\delta}_R+\begin{pmatrix}e^{-i\omega_s\tau}&0&0\\0&e^{i\omega_s\tau}&0\\0&0&0\end{pmatrix}$$

$$\times[h_y^x\vec{\delta}_R(t-\tau)-f_y^x\vec{\delta}_R],$$

with $f_y^x=(X/\tau_c)(m_+\pm c_-)$, $h_y^x=(X/\tau_c)(m_+\mp c_-)$ with the upper sign for x and the lower sign for y.

$$c_1=\Gamma G_N(1+i\alpha)e_+, \quad j_1=\left(\frac{1}{\tau_e}+\Gamma G_N e_+^2\right),$$

$$j_2=\left(\frac{1}{\tau_s}+\Gamma G_N e_+^2\right), \quad c_2=\pm 2(\gamma_a+i\gamma_b),$$

$$j_0=\tfrac{1}{2}\Gamma G_N(N_s-N_0)e_+$$
$$=\tfrac{1}{2}\Gamma G_N(N_{\rm th}-N_0)e_+ +[\pm\gamma_a-f_y^x\cos(\omega_s\tau)]e_+ .$$

If $\theta=\pi/2$,

$$f_y^x=\frac{X}{\tau_c}(m_+\pm c_-)=\frac{X}{\tau_c}\begin{cases}0 & \text{polarization } x\\ 1 & \text{polarization } y\end{cases},$$

$$h_y^x=\frac{X}{\tau_c}\begin{cases}1 & \text{polarization } x\\ 0 & \text{polarization } y\end{cases}.$$

γ_a is the dichroism, γ_b the birefringence, Γ the confinement factor, G_N the differential gain, N_0 the carrier number at transparency, $N_{\rm th}$ the carrier number at threshold, τ_s the relaxation time of the spin interaction, τ_e the carrier relaxation time, α the phase-amplitude factor, X/τ_c the feedback rate, $m_+=m_-$, $c_-=c_+$, respectively, the diagonal and the off-diagonal coefficients of the associated Jones matrix of the external cavity.

One should note that when the feedback light is polarized along y (respectively, x), the component R which describes the evolution of small deviations from the stationary solutions linearly polarized along x is submitted to a delayed term. The spin relaxation couples both linearly polarized components and delayed terms.

The first system gives the following characteristic equation:

$$(e^{-\lambda\tau}-1)f_x^y\left[(e^{-\lambda\tau}-1)f_x^y\frac{(P-N_0/\tau_e)}{(N_s-N_0)}-\Gamma G_N\left(P-\frac{N_s}{\tau_e}\right)\right.$$
$$\left.\times[\cos(\omega_s\tau)-\alpha\sin(\omega_s\tau)]\right]+\lambda\left[(e^{-\lambda\tau}-1)^2 f_x^{y\,2}\right.$$
$$+\Gamma G_N\left(P-\frac{N_s}{\tau_e}\right)-2(e^{-\lambda\tau}-1)f_x^y\frac{(P-N_0/\tau_e)}{(N_s-N_0)}$$
$$\left.\times\cos(\omega_s\tau)\right]+\lambda^2\left[\frac{(P-N_0/\tau_e)}{(N_s-N_0)}-2(e^{-\lambda\tau}-1)\right.$$
$$\left.\times f_x^y\cos(\omega_s\tau)\right]+\lambda^3=0$$

while the equation of the second system is written

$$c(a^2+b^2)-\Gamma G_N\left(P-\frac{N_s}{\tau_e}\right)(a+\alpha b)+\lambda\left[a^2+b^2\right.$$
$$\left.+\Gamma G_N\left(P-\frac{N_s}{\tau_e}\right)-2ac\right]+\lambda^2(c-2a)+\lambda^3=0,$$

with

$$a=[\pm 2\gamma_a+(h_x^y e^{-\lambda\tau}-f_x^y)\cos(\omega_s\tau)],$$

$$b=[\pm 2\gamma_b-[h_x^y e^{-\lambda\tau}-f_x^y]\sin(\omega_s\tau)],$$

$$c=\left(\frac{1}{\tau_s}+\frac{(P-N_0/\tau_e)}{(N_s-N_0)}\right).$$

These equations are solved for λ. Stability diagrams like those of Ref. [34] are obtained. The border separating stable [$\mathrm{Re}(\lambda)<0$] from unstable region [$\mathrm{Re}(\lambda)>0$] is obtained by setting $\mathrm{Re}(\lambda)=0$. N_0 has a small influence on these diagrams and will slightly modify the curves which limit the regions of stability. The critical parameter values for the parameter in the stability diagram of Ref. [34] are given by

$$\frac{P}{P_{\rm th}}<\frac{P_x}{P_{\rm th}}=1+\frac{\tau_e}{\tau_s}\frac{\gamma_b}{[\alpha\Gamma G_N N_{\rm th}/2-\gamma_b N_{\rm th}/(N_{\rm th}-N_0)]}$$
$$=2.5 \quad (\gamma_b=16\ \text{GHz}),$$

$$\frac{P}{P_{\rm th}}>\frac{P_y}{P_{\rm th}}=1-\left(1-\frac{N_0}{N_{\rm th}}\right)\frac{\tau_e}{\tau_s}+2\alpha\left(1-\frac{N_0}{N_{\rm th}}\right)\frac{\tau_e}{\tau_p}\gamma_b .$$

Only the y-stability condition is effectively changed by the insertion of the carrier at transparency. The value of γ_b for which $P_y/P_{\rm th}=1$ is given by the same value as in Ref. [34]: $\gamma_b=1/2\alpha\tau_s=13.15$ GHz. τ_s has been taken equal to 10 ps in order to get a quite high value of $1/2\alpha\tau_s=13.15$ GHz, the limit above which only the x-polarized mode is stable.

According to the linear stability analysis, when there is no amplitude anisotropy, the laser should operate in the third region (x stable region) in order to get a frequency shift of 10–13 GHz. One could note that for some lasers with different anisotropies, both modes were stable close to the threshold, which means $\gamma_a>0$. For higher values of the bias current ($P/P_{\rm th}>1.03$), only one polarized mode was stable. This was not the case for the presented results. For all tested components, only one polarized mode was stable above threshold. For $P/P_{\rm th}$ above 1.5–1.8 (depending on the components), the laser has several transverse modes.

[1] W. Culshaw and J. Kannelaud, Phys. Rev. **156**, A308 (1967).
[2] Y. C. Chen and J. M. Liu, Opt. Quantum Electron. **19**, 93 (1987).
[3] J. M. Liu and Y. C. Chen, IEEE J. Quantum Electron. **21**, 298 (1985).
[4] A. W. Lohman, Appl. Phys. Lett. **25**, 298 (1986).
[5] A. Klehr, R. Müller, M. Voss, and A. Bärwolff, Appl. Phys. Lett. **64**, 830 (1994).
[6] Toshihiko Ouchi, Masao Majima, Sotomitsu Ikeda, Takeo Ono, Mamoru Uchida, and Yuici Handa, Appl. Phys. Lett. **67**, 3405 (1995).
[7] Matsuto Ogawa, Electron. Commun. Jpn. 2, Electron. **78**,

46 (1995).
[8] D. G. H. Nugent, R. G. S. Plumb, M. A. Fisher, and D. A. O. Davies, Electron. Lett. **31**, 43 (1995).
[9] A. Sapia, P. Spano, and B. Daino, Appl. Phys. Lett. **50**, 57 (1987).
[10] H. Kawaguchi and I. S. Hidayat, Electron. Lett. **31**, 1150 (1995).
[11] T. Fujita, A. Schremer, and C. L. Tang, Appl. Phys. Lett. **61**, 392 (1987).
[12] D. Syvridis, D. Inaudi, and G. Guekos, IEEE J. Quantum Electron. **30**, 966 (1994).
[13] S. Pajarola, G. Guekos, and J. Mork, IEEE Photonics Technol. Lett. **8**, 157 (1996).
[14] Tsuyoshi Toda, Nagaatsu Ogasawara, and Ryoichi Ito, Jpn. J. Appl. Phys., Part 1 **27**, 1702 (1988).
[15] K. D. Choquette, K. L. Lear, R. E. Leibenguth, and M. T. Asom, Appl. Phys. Lett. **64**, 2767 (1994).
[16] Z. G. Pan, Shijun Jiang, and M. Dagenais, Appl. Phys. Lett. **63**, 2999 (1993).
[17] T. Mukaihara, N. Ohnoki, Y. Hayashi, N. Hatori, F. Koyama, and K. Iga, IEEE Photonics Technol. Lett. **7**, 1113 (1995).
[18] E. Goobar, J. W. Scott, B. Thibeault, G. Robinson, Y. Akulova, and L. A. Coldren, Appl. Phys. Lett. **67**, 3697 (1995).
[19] D. V. Kuksenkov and H. Temkin, Appl. Phys. Lett. **67**, 2141 (1995).
[20] K. D. Choquette, R. P. Schneider, Jr., K. L. Lear, and R. E. Leibenguth, IEEE J. Sel. Top. Quantum Electron. **1**, 661 (1995).
[21] T. Mukaihara, N. Onhoki, Y. Hayashi, N. Hatori, F. Koyama, and K. Iga, IEEE J. Sel. Top. Quantum Electron. **1**, 667 (1995).
[22] J-H. Ser, Y-G. Ju, J-H Shin, and Y. H. Lee, Appl. Phys. Lett. **66**, 2769 (1995).
[23] T. Numai, K. Kurihara, K. Kühn, H. Kosaka, I. Ogura, M. Kajita, H. Saito, and K. Kasahara, IEEE J. Quantum Electron. **31**, 636 (1995).
[24] Dacai Sun, E. Towe, P. H. Ostdiek, J. W. Grantham, and G. J. Vansuch, IEEE J. Sel. Top. Quantum Electron. **1**, 674 (1995).
[25] D. Vakshoori and R. E. Leibenguth, Appl. Phys. Lett. **67**, 1045 (1995).
[26] D. Vakshoori, Appl. Phys. Lett. **65**, 259 (1994).
[27] A. D. May and G. Stephan, J. Opt. Soc. Am. B **6**, 2355 (1989).
[28] P. Besnard, Xiaolin Jia, R. Dalgliiesh, A. D. May, and G. Stéphan, J. Opt. Soc. Am. B **10**, 1605 (1993).
[29] F. Robert, P. Besnard, G. Stephan, D. Vakhshoori, P. Paddon, and A. D. May, Tech. Dig. Cleo Europe **1994**, 353.
[30] F. Robert, P. Besnard, M. L. Charès, and G. M. Stéphan, Opt. Quantum Electron. **27**, 805 (1995). Note the misprint: one should read 12.81 GHz instead of 2.81 GHz.
[31] M. San Miguel, Q. Feng, and J. V. Moloney, Phys. Rev. A **52**, 1728 (1995).
[32] R. A. Morgan, L. M. Chirovsky, M. W. Focht, G. Guth, M. T. Asom, R. E. Leibenguth, K. C. Robinson, Y. H. Lee, and J. L. Jewell, Proc. SPIE **1562**, 149 (1991).
[33] Shijun Jiang, Zeqi Pan, M. Dagenais, R. A. Morgan, and K. Kojima, Appl. Phys. Lett. **63**, 3545 (1993).
[34] J. Martin-Regalado, F. Prati, M. San Miguel, and N. B. Abraham, IEEE J. Quantum Electron. **33**, 765 (1997).
[35] F. Robert, P. Besnard, M. L. Charès, and G. M. Stéphan, IEE Proc.: Optoelectron. **143**, 104 (1996).
[36] P. Besnard, B. Meziane, and G. Stéphan, IEEE J. Quantum Electron. **29**, 1271 (1993).
[37] S. Jiang, Z. Pan, M. Dagenais, R. A. Morgan, and K. Kojima, IEEE Photonics Technol. Lett. **6**, 34 (1994).
[38] S. Jiang, M. Dagenais, and R. A. Morgan, IEEE Photonics Technol. Lett. **7**, 739 (1995).
[39] K. Peterman, IEEE J. Sel. Top. Quantum Electron. **1**, 480 (1995).
[40] G. H. M. van Tartwijk and D. Lenstra, Quantum Semiclassic. Opt. **7**, 87 (1995).
[41] U. Fiedler and K. J. Ebeling, IEEE J. Sel. Top. Quantum Electron. **1**, 442 (1995).
[42] R. W. Tkach and A. R. Chraplyvy, J. Lightwave Technol. **4**, 1655 (1986).
[43] K. Petermann, *Laser Diode Modulation and Noise* (Kluwer, Dordrecht, 1988), p. 124.
[44] Dag Roar Hjelme and Alan Rolf Mickelson, IEEE J. Quantum Electron. **25**, 1625 (1989).
[45] M. Yamada, IEEE J. Quantum Electron. **19**, 1365 (1983).
[46] DuBravko I. Babic and Scott W. Corzine, IEEE J. Quantum Electron. **28**, 514 (1992).
[47] J. H. Osmundsen and N. Gade, IEEE J. Quantum Electron. **19**, 465 (1983).
[48] R. C. Jones, J. Opt. Soc. Am. **38**, 671 (1948).
[49] F. Robert, P. Besnard, M-L. Chares, and G. Stephan (unpublished).
[50] F. Robert, Ph.D. thesis, 1997.
[51] J. W. Bae and H. Temkin, Appl. Phys. Lett. **63**, 1480 (1993).
[52] G. A. Acket, D. Lenstra, A. J. Den Boef, and B. H. Verbeek, IEEE J. Quantum Electron. **20**, 1163 (1984).
[53] H. Kawaguchi, *Bistabilities and Nonlinearities in Laser Diodes* (Artech House, Boston, 1994), p. 148.
[54] C. Z. Ning, R. A. Indik, and J. V. Moloney, J. Opt. Soc. Am. B **12**, 1993 (1995).
[55] W. W. Chow, S. W. Koch, and M. Sargent III, *Semiconductor-laser Physics* (Springer-Verlag, Berlin, 1994).